treme case of a conformational effect on ET. This conformational effect is expressed as the effect of the protein's secondary structure on the rate of long-range electron transfer (*23*).

An alternative perspective on this mechanism arises from a solid-state origin. For the all trans configuration a periodicity exists in the chain, and one can consider the bonding and antibonding orbitals, resulting in a nascent valence band and conduction band, respectively (*24*). In this case, the molecular states through which the coupling occurs are fully delocalized over the chain units. The tunneling of the charge through the layer may be considered as the migration of the electron mediated by the conduction band or as the migration of the hole by way of the valence band. When the chains become disordered, the periodicity (or the symmetry) is broken and the orbitals are less delocalized. Either of these viewpoints appears valid, and it seems likely that they are equivalent.

The large decrease in the reverse current, when OTS covers the electrode, reflects the presence of a wider, and perhaps higher, barrier than is present with just the oxide overlayer on the electrode. In principle, ET between the silicon and the electrolyte can occur either through the HOMO or the LUMO of the intervening phase. When the energy of the electron donating, of the electron accepting, or of both states lies closer to the HOMO than to the LUMO, coupling through the HOMO by way of the hole mechanism should dominate. Because the energy of the valence band edge is closer to the HOMO than to the LUMO, it is likely that this mechanism dominates the hole transfer (reverse current under illumination) and that the LUMO mechanism dominates the electron transfer (forward current).

Alternatively, the shifts in the onset voltage may reflect properties of the oxide layer as much as those of the alkane layer. In particular, defect states in the oxide layer of the electrode may mediate the forward current. Addition of the OTS may block this pathway for the forward current. In this scenario, the charge transfer through the alkane layers could be a mixture of the HOMO and LUMO mechanisms. The results reflect, therefore, the weaker coupling of the LUMO to the defect states of the oxide. Both of these explanations are consistent with the data.

The present experiment demonstrates the important role of symmetry (or periodicity) in the determination of electronic coupling and hence ET efficiency. These results clearly show that the ordered, all trans monolayer has a higher charge transfer efficiency than a disordered monolayer. Furthermore, the data suggest a hole mechanism for the electronic coupling.

Note added in proof: Recently a theoretical analysis of ET (*5*) showed that, for small energy differences between donor and acceptor, a complex distance dependence results. Such a dependence is predicted to be sensitive to the properties of the bridging material. Our results present direct experimental evidence for such sensitivity.

REFERENCES AND NOTES

1. R. A. Marcus and N. Sutin, *Biochim. Biophys. Acta* **811**, 265 (1985); D. N. Beratan, J. N. Onuchic, J. R. Winkler, H. B. Gray, *Science* **258**, 1740 (1992), and references therein.
2. M. D. Newton, *Chem. Rev.* **91**, 767 (1991).
3. C. Liang and M. D. Newton, *J. Phys. Chem.* **96**, 2855 (1992); *ibid.* **97**, 3199 (1993).
4. L. A. Curtiss, C. A. Naleway, J. R. Miller, *Chem. Phys.* **176**, 387 (1993).
5. J. W. Evenson and M. Karplus, *Science* **262**, 1247 (1993).
6. E. E. Polymeropoulos, D. Mobius, H. Kuhn, *J. Chem. Phys.* **68**, 3918 (1978); *Thin Solid Films* **68**, 173 (1980).
7. C. E. D. Chidsey, *Science* **251**, 919 (1991).
8. P. C. Vincett and G. G. Roberts, *Thin Solid Films*, **68**, 135 (1980).
9. M. N. Paddon-Row, *Acc. Chem. Res.* **15**, 245 (1982).
10. C. Miller, P. Cuendet, M. Gratzel, *J. Phys. Chem.* **95**, 877 (1991); A. B. Becka and C. J. Miller, *ibid.* **96**, 2657 (1992).
11. M. A. Ratner, *ibid.* **94**, 4877 (1990).
12. K. D. Jordan and M. N. Paddon-Raw, *Chem. Rev.* **92**, 395 (1992).
13. H. Kuhn, *J. Photochem.* **10**, 11 (1972).
14. R. J. Behm, N. Garcia, H. Roher, Eds., *Scanning Tunneling Microscopy and Related Methods* (Kluwer Academic, Norwell, MA, 1990), p. 377.
15. R. Maoz and J. Sagiv, *J. Colloid Interface Sci.* **101**, 201 (1984).
16. Y. Paz, S. Trakhtenberg, R. Naaman, *J. Phys. Chem.* **96**, 10964 (1992).
17. A. Ulman, *An Introduction to Ultrathin Organic Films* (Academic Press, New York, 1991), p. 256.
18. L. J. Huang and W. M. Lau, *J. Vac. Sci. Technol. A* **10**, 812 (1992); M. Niwano *et al.*, *ibid.*, p. 3171.
19. S. R. Morrison, *Electrochemistry at Semiconductor and Oxidized Metal Electrodes* (Plenum, New York, 1984); N. S. Lewis, *Annu. Rev. Phys. Chem.* **42**, 543 (1991); C. A. Koval and J. N. Howard, *Chem. Rev.* **92**, 411 (1992).
20. H. M. McConnell, *J. Chem. Phys.* **35**, 508 (1961).
21. R. Hoffmann, *Acc. Chem. Res.* **4**, 1 (1971); ———, A. Imamura, J. Hehre, *J. Am. Chem. Soc.* **90**, 1499 (1967).
22. D. N. Beratan, J. N. Onuchic, J. N. Betts, B. E. Bowler, H. B. Gray, *J. Am. Chem. Soc.* **112**, 7915 (1990).
23. D. N. Beratan and J. N. Onuchic, *Adv. Chem.* **228**, 71 (1990).
24. W. A. Harrison, *Electronic Structure and the Properties of Solids* (Freeman, New York, 1980).

25. We thank K. Jordan and D. Beratan for useful discussions. Supported by the MINERVA Foundation and the Israel Science Foundation (R.N.), the U.S. Department of Energy (D.H.W.), and the Israel National Council on Research and Development and the KFA Jülich (Germany) (D.C.).

28 September 1993; accepted 15 December 1993

Crystal Structure, Bonding, and Phase Transition of the Superconducting Na_2CsC_{60} Fulleride

Kosmas Prassides,* Christos Christides, Ian M. Thomas, Junichiro Mizuki, Katsumi Tanigaki,* Ichiro Hirosawa, Thomas W. Ebbesen

The crystal structure of superconducting Na_2CsC_{60} was studied by high-resolution powder neutron diffraction between 1.6 and 425 K. Contrary to the literature, the structure at low temperatures is primitive cubic ($Pa\bar{3}$), isostructural with pristine C_{60}. Anticlockwise rotation of the C_{60} units by 98° about [111] allows simultaneous optimization of C_{60}-C_{60} and alkali-fulleride interactions. Optimal Na^+-C_{60}^{3-} coordination is achieved with each sodium ion located above one hexagon face and three hexagon-hexagon fusions of neighboring fulleride ions (coordination number 12). Reduction of the C_{60} molecule lengthens the hexagon-hexagon fusions and shortens the pentagon-hexagon fusions (to ~1.43 angstroms). On heating, Na_2CsC_{60} undergoes a phase transition to a face-centered-cubic $Fm\bar{3}m$ phase, best modeled as containing quasi-spherical C_{60}^{3-} ions. The modified structure and intermolecular potential provide an additional dimension to the behavior of superconducting fullerides and should sensitively affect their electronic and conducting properties.

Superconducting alkali metal fullerides (*1*) with stoichiometry A_3C_{60} (A = K, Rb) adopt a merohedrally disordered face-centered-cubic (fcc) structure (*2*) ($Fm\bar{3}m$). In these solids, each C_{60}^{3-} ion is located at an fcc lattice site and is randomly distributed between two orientations related by 90° rotations about the cubic [001] directions. This type of structural disorder is recognized as being principally responsible for many of the electronic properties of these systems (*3*, *4*), with a close connection existing between the orientational state of A_3C_{60} and its superconducting properties. Superconductivity in the fullerenes has been

K. Prassides, C. Christides, I. M. Thomas, School of Chemistry and Molecular Sciences, University of Sussex, Brighton BN1 9QJ, United Kingdom.
J. Mizuki, K. Tanigaki, I. Hirosawa, T. W. Ebbesen, Fundamental Research Laboratories, NEC Corporation, 34 Miyukigaoka, Tsukuba 305, Japan.
*To whom correspondence should be addressed.

explained by both conventional electron-phonon (5) and purely electronic (6) models. In both models, pair binding is assumed to be dominated by intramolecular properties. Moreover, the observed monotonic scaling of the superconducting critical temperature (T_c) with the unit cell size (7) was rationalized as arising, to first order, from the modulation of the electronic density of states by the interfullerene spacing.

Deviations from this behavior were first noted for fullerides intercalated with the small Na^+ ions (8, 9). The experimental observation of phase separation in Na_3C_{60} on cooling offered an explanation for the lack of superconductivity in this fulleride (8). However, the case of Na_2RbC_{60}, which has a much lower than expected T_c of ~3.5 K (9), is more subtle and has remained unexplained. Small deviations of the intensities of x-ray reflections from the predictions of the merohedral disorder structural model led to the suggestion (10) that additional rotational disorder was responsible for the anomalous T_c. A subsequent high-resolution synchrotron study of Na_2RbC_{60} showed, however, the presence of weak Bragg peaks that could be indexed (11) as primitive cubic (space group $Pa\bar{3}$) but not as fcc. This observation, coupled with the presence of fullerene orientational ordering in lightly doped Na_xC_{60} ($x \sim 1.3$) (12), has led to the possibility that the additional degrees of orientational freedom associated with the primitive cubic structure may have a detrimental effect on the superconducting properties of Na_2RbC_{60}.

In this report, we address the problem of the structure of the ternary fulleride Na_2CsC_{60}. This compound has both a T_c and a lattice constant entirely consistent with the universal curve of fcc fullerides. We probed its structural properties between 1.6 and 425 K by high-resolution powder neutron diffraction. Unexpectedly, we found that its crystal structure at low temperatures is not fcc but primitive cubic ($Pa\bar{3}$), isostructural with pristine C_{60} (13). Moreover, no discernible structural change occurs on heating through T_c. Thus, even though the presence of changed orientational ordering should have modified the density of states at the Fermi surface and, as a consequence, T_c, no such effect was apparent. This poses a stringent test for any model of superconductivity in these materials, which should predict correctly the effects of both the lowering of symmetry and the relative intermolecular orientations of C_{60} on the band structure at the Fermi surface.

The Na_2CsC_{60} sample was prepared by reaction of stoichiometric quantities of C_{60}, Na, and Cs contained in a tantalum cell inside a sealed glass tube filled with He to 600 torr at 200°C for 12 hours and at 430°C for 3 weeks with intermittent shaking. Phase purity was confirmed by x-ray diffraction. The sample was superconducting (14) with T_c = 12 K and a superconducting volume fraction of 59%. For the neutron diffraction measurements, the 500-mg sample was placed in a flat aluminium sample holder with thin vanadium windows and was press sealed with gold wire. With the sample inside a continuous-flow cryostat, neutron powder diffraction data were collected at 1.6, 20, and 425 K with the high-resolution powder diffractometer at the ISIS facility, Rutherford Appleton Laboratory, United Kingdom. The sample was placed at the low-resolution ($\Delta d/d = 8 \times 10^{-4}$) high-flux position. The d-spacing range extended from 0.93 to 3.3 Å (1.6 and 425 K) and from 0.93 to 2.3 Å (20 K). Data analysis was performed with the ISIS powder diffraction software.

Inspection of the diffraction profile at 1.6 K (Fig. 1) readily reveals a number of reflections that index to primitive cubic symmetry, violating fcc rules. Rietveld refinements (Table 1) were then performed with the primitive cubic space group $Pa\bar{3}$ as systematic absences of reflections necessitated. In a fashion analogous to pristine C_{60} (13), the four C_{60}^{3-} ions in the unit cell were allowed to rotate anticlockwise in a stepwise manner by an arbitrary angle ϕ (in multiples of $\delta\phi = 4°$ between $\phi = 0°$ and 120°) about the [111] direction. The result-

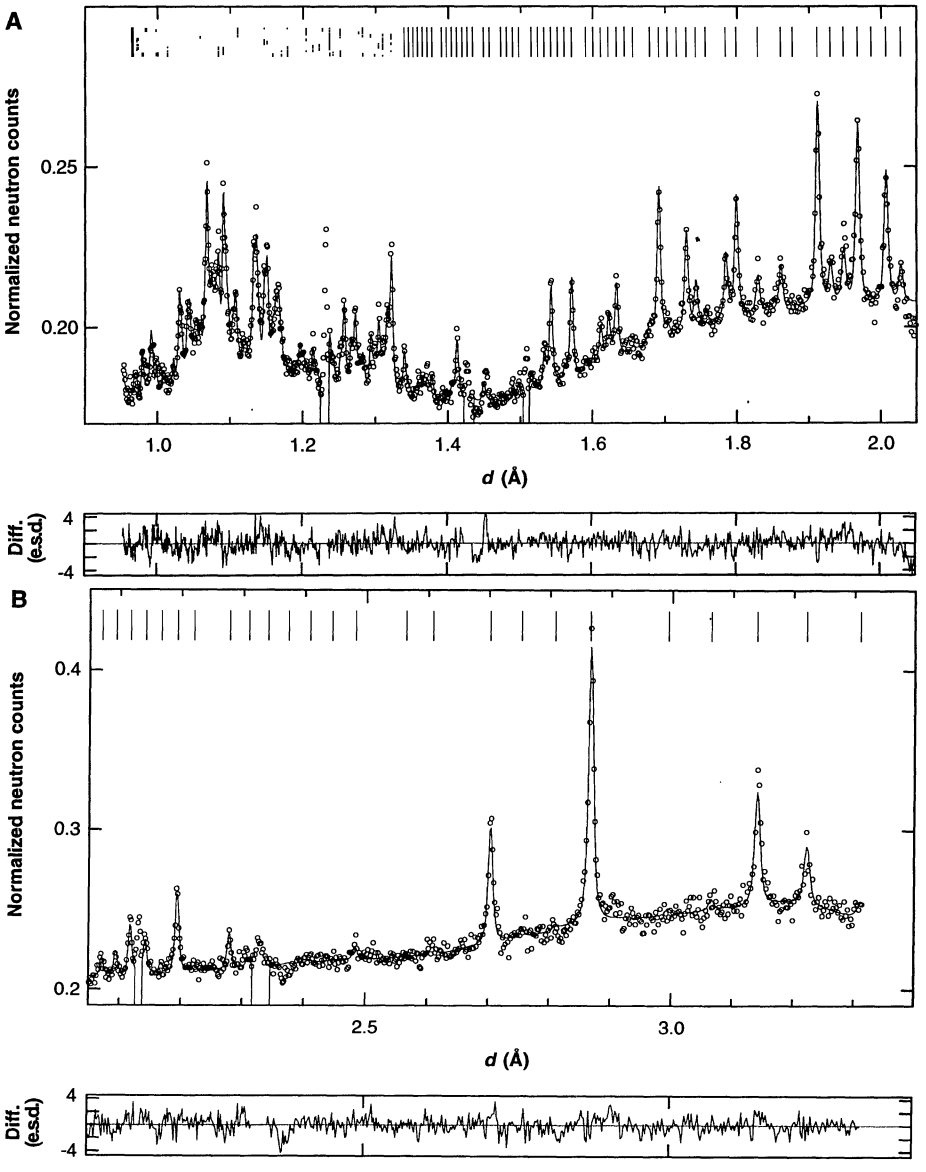

Fig. 1. Final observed (points) and calculated (solid line) diffraction profile for Na_2CsC_{60} at 1.6 K in the region (**A**) d = 0.95 to 2.05 Å and (**B**) d = 2.05 to 3.30 Å. The lower panels show the difference profile in units of estimated standard deviations (e.s.d.). Some regions contaminated with vanadium and aluminum reflections were excluded from the refinement. Marks at top of each figure marked the observed reflections.

ing χ^2 values clearly establish $Pa\bar{3}$ as the correct choice, with a deep minimum in χ^2 (~2.7) at $\phi \approx 98°$, exactly as in C_{60}. Subsequent refinements were thus performed in $Pa\bar{3}$ with starting coordinates for C_{60}^{3-} corresponding to this particular rotation and Na^+ and Cs^+ ions placed in tetrahedral and octahedral holes, respectively. The C_{60} positional parameters were varied subject to restraints of ±0.010 Å on the lengths of three sets of C–C bonds (one set of hexagon-hexagon and two sets of hexagon-pentagon fusions) and of ±0.10° on the pentagon and hexagon angles. Moreover, the space group $Pa\bar{3}$ allows the displacement of the Na^+ ions (local symmetry C_3) from the ideal tetrahedral position along the [111] cube diagonals. Stable refinement was quickly achieved, but even though agreement between observed and calculated profiles became very good, there were signs of systematic differences between model and experimental intensities reminiscent of the situation in C_{60} (*15*). Examination of the χ^2 evolution with rotation angle ϕ showed the presence of a second broad plateau at $\chi^2 \approx 12$ extending from $\phi = 22°$ to 62°. We thus decided to introduce in the refinement a second orientation for C_{60} units, corresponding to a rotation angle of 38°. The Rietveld refinement immediately improved significantly with the fraction of the C_{60}^{3-} ions at ~98° converging to 88.3(8)% (the number in parentheses is the error in the last digit) and a final $\chi^2 = 1.7$. The projection of the structure on the basal plane of the unit cell is shown in Fig. 2A. The diffraction pattern recorded above T_c, at 20 K, was also refined with the same two-state $Pa\bar{3}$ model. No discernible differences are evident between 1.6 and 20 K. The lattice constant is $a = 14.0464(2)$ Å, compared with $a = 14.0458(2)$ Å at 1.6 K, and the fraction of the molecules in the major orientation is virtually unchanged at 88.1(8)%.

The use of a gold seal to protect the air-sensitive sample from exposure to air also allowed us to heat it inside the cryostat to a temperature of 425 K. The diffraction data collected at this temperature were drastically different. The peaks at low *d* were distinctly weaker in intensity, and the reflections indicated fcc symmetry. Rietveld refinements were attempted with both the merohedral disorder ($Fm\bar{3}m$) and the single C_{60} orientation ($Fm\bar{3}$) models. The agreement between these models and the measured profiles is unsatisfactory. In view of the similarity with the behavior of pristine C_{60} at low temperatures, we considered a structural model (space group $Fm\bar{3}m$) in which, to a first approximation, the C_{60}^{3-} ions were taken as uniform spherical units (*16*) and the Na^+ and Cs^+ ions were placed in the ideal tetrahedral and octahedral positions, respectively. Simulations of the powder diffraction profile, with use of a radius of 3.54 Å for the C_{60}^{3-} ions, agree with the observed data (Fig. 3), resulting in an integrated intensities χ^2 value of 2.8 (compare with $\chi^2 = 10.2$ for the merohedrally disordered $Fm\bar{3}m$ mod-

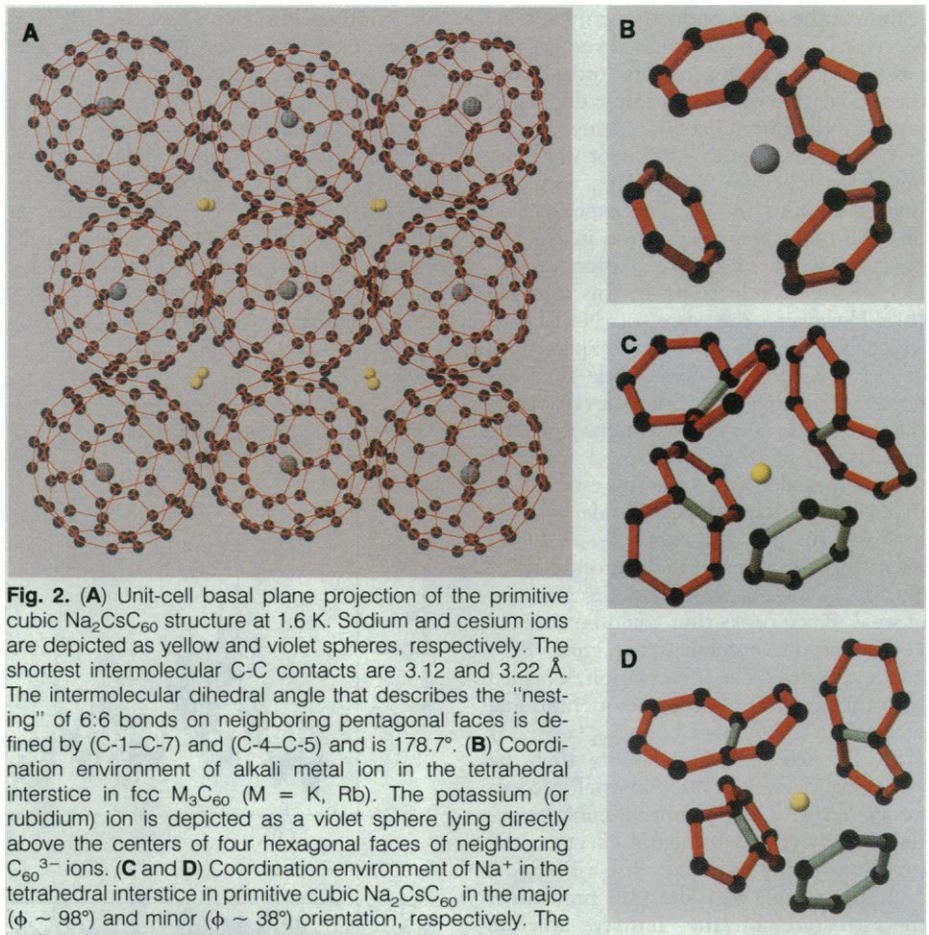

Fig. 2. (**A**) Unit-cell basal plane projection of the primitive cubic Na_2CsC_{60} structure at 1.6 K. Sodium and cesium ions are depicted as yellow and violet spheres, respectively. The shortest intermolecular C-C contacts are 3.12 and 3.22 Å. The intermolecular dihedral angle that describes the "nesting" of 6:6 bonds on neighboring pentagonal faces is defined by (C-1–C-7) and (C-4–C-5) and is 178.7°. (**B**) Coordination environment of alkali metal ion in the tetrahedral interstice in fcc M_3C_{60} (M = K, Rb). The potassium (or rubidium) ion is depicted as a violet sphere lying directly above the centers of four hexagonal faces of neighboring C_{60}^{3-} ions. (**C** and **D**) Coordination environment of Na^+ in the tetrahedral interstice in primitive cubic Na_2CsC_{60} in the major ($\phi \sim 98°$) and minor ($\phi \sim 38°$) orientation, respectively. The sodium ions are depicted as yellow spheres lying directly above the center of a hexagonal face and the midpoints of three 6:6 (major fraction) or 6:5 (minor fraction) bonds of neighboring C_{60}^{3-} ions. The nearest C–C bonds to the Na^+ ions are shown in green.

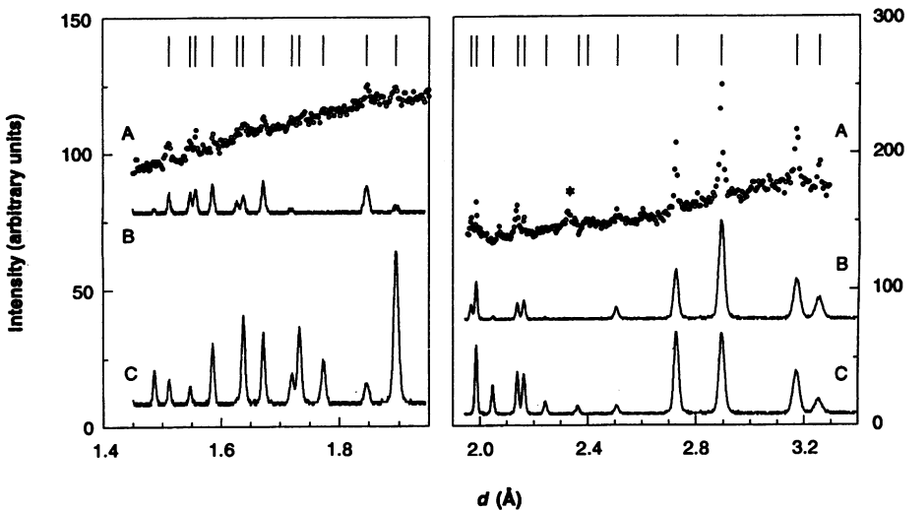

Fig. 3. Diffraction profile for Na_2CsC_{60} at 425 K (A), shown with simulations using space group $Fm\bar{3}m$ for a spherically (B) and a merohedrally (C) disordered model for C_{60} in the range $1.45 < d < 3.3$ Å. An aluminum peak is marked by the (*).

el). Deviations from perfect spherical symmetry, as it has been described for pristine C_{60} in its high-temperature phase (*17*), are expected and might be revealed by a symmetry-adapted spherical-harmonics description of the orientational distribution function of the fullerene units. The refined lattice constant at 425 K is 14.1819(7) Å, yielding a 0.969(6)% expansion between 1.6 and 425 K. This is similar to the expansion of 0.875(6)% for pristine C_{60} between 5 and 320 K and implies the existence of a lattice constant jump at the first-order phase transition from primitive cubic to fcc for Na_2CsC_{60}.

Several points arising from the results of the present refinements are of particular interest. The C–C bonds fusing two hexagons (6:6) lengthened [average value, 1.43(1) Å] and the ones fusing a hexagon and a pentagon (6:5) have shortened [average, 1.43(1) Å] substantially compared with C_{60} [1.39(2) and 1.45(1) Å, respectively], to the point that they are indistinguishable within the experimental error of the present study. Such experimental information is crucial in the calculation of accurate electron-molecular vibration coupling constants, which are used in Bardeen-Cooper-Schrieffer (BCS)–type models of superconductivity in the fullerides. Smoothing out of the bond length alternation on reduction has been anticipated by the results of theoretical studies (*18*) with the role of the crystalline field arising from the intercalated ions expected to be significant.

As a result of the orientational ordering of the C_{60}^{3-} ions, the coordination number of the alkali ion in the tetrahedral interstice has been reduced from 24 in merohedrally disordered K_3C_{60} to 12 in Na_2CsC_{60}. In combination with its small ionic radius (0.95 Å), this allows the Na^+ ions to be closer to the hexagonal face of an adjacent C_{60} [2.98(3) Å for the dominant orientation] (Fig. 2C), thereby leaving enough space for the other three neighboring C_{60}^{3-} ions to rotate in such a way as to optimize the C_{60}-C_{60} interactions. For the rotation angle of ~98°, at which 6:6 fusions of C_{60} become parallel to pentagonal faces of the adjacent molecules, the Na^+-C_{60}^{3-} contacts assume a highly optimal configuration (Fig. 2C); namely, the cation is directly above 6:6 fusions, the very same configuration that is adopted by the ions in the octahedral holes of the merohedrally disordered fullerides. This probably contributes to the observed lengthening of the C_{60}^{3-} 6:6 fusions. The Cs^+ ions that occupy the large octahedral holes are located above 6:5 fusions. Despite the closer approach between C_{60}^{3-} and Na^+, the contacts [2.72(3) and 2.85(3) Å for the dominant orientation] are still larger than the sum of the ionic radius of Na^+ and the van der Waals radius of C. We also present for comparison (Fig. 2B) the coordination of the ion in the tetrahedral hole in the merohedrally disordered fcc fullerides.

For the minor configuration ($\phi \approx 38°$) (Fig. 2D), Na^+ coordinates to three 6:5 fusions as well as to the C atoms of a hexagonal face, a situation somewhat less energetically favorable. In combination with the less favorable C_{60}-C_{60} contacts for this rotation angle, this results in only 11.3(8)% fractional occupation of this orientation at 1.6 K. The difference in energy between the global and local minima should thus be somewhat larger than the value of 11.4(3) meV (*19*) found in C_{60}. The similarity in structural behavior with pristine C_{60} and the occurrence of the primitive cubic-to-fcc phase transition implies the existence in Na_2CsC_{60} of a rotational potential more similar to C_{60} than to K_3C_{60} or Rb_3C_{60}. Neutron inelastic scattering measurements (*20*) on Na_2RbC_{60} in the orientationally ordered phase reveal the presence of librations of energy around ~2.8 meV (at 50 K). These are slightly harder than those in C_{60} and lead to an estimate for the rotational activation barrier in ternary sodium fullerides of the order of 300 meV, much lower than the 500 meV

Table 1. Fractional atomic coordinates (*x*, *y*, *z*) for Na_2CsC_{60} obtained from Rietveld refinement at 1.6 K. Estimated errors in last digit are given in parentheses. The neutron scattering lengths of C, Na, and Cs are 6.648, 3.63, and 5.42 fm, respectively. The space group is $Pa\bar{3}$ and the lattice constant a = 14.0458(2) Å. The weighted profile and expected R factors are R_{wp} = 1.3% and R_E = 1.0%; the background-excluded values are R_{wp} = 6.7% and R_E = 5.2%. The background was described by a 20-term Chebychev polynomial. The thermal factors were handled as an overall temperature factor, which refined to 0.3(1) Å^2. Fractional occupancies of C atoms in the major orientation (C-1 to C-10) are 0.883(8). The coordinates of the atoms in the minor [0.117(8)] fraction (C-1* to C-10*) were evaluated by rotation of each C atom in the major fraction by 60° anticlockwise about [111].

Atom	Site	*x/a*	*y/a*	*z/a*
Cs	4b	0.5	0.5	0.5
Na	8c	0.241(1)	0.241(1)	0.241(1)
		Major orientation		
C-1	24d	0.2265(3)	−0.0342(3)	0.1065(4)
C-2	24d	0.2455(3)	−0.0581(3)	0.0090(3)
C-3	24d	0.2063(3)	0.0620(3)	0.1322(4)
C-4	24d	0.2051(3)	−0.1429(3)	−0.0314(3)
C-5	24d	0.1673(3)	−0.0953(3)	0.1635(3)
C-6	24d	0.2441(3)	0.0140(3)	−0.0620(3)
C-7	24d	0.2051(3)	0.1345(4)	0.0609(3)
C-8	24d	0.1462(3)	−0.2039(3)	0.0261(3)
C-9	24d	0.1273(3)	−0.1801(3)	0.1229(3)
C-10	24d	0.2240(3)	0.1107(3)	−0.0362(3)
		Minor orientation		
C-1*	24d	0.0927(3)	−0.0273(3)	0.2334(4)
C-2*	24d	0.1219(3)	−0.1145(3)	0.1890(3)
C-3*	24d	0.1348(3)	0.0607(3)	0.2050(4)
C-4*	24d	0.0519(3)	−0.1845(3)	0.1635(3)
C-5*	24d	−0.0065(3)	−0.0103(3)	0.2524(3)
C-6*	24d	0.1928(3)	−0.1134(3)	0.1168(3)
C-7*	24d	0.2061(3)	0.0619(4)	0.1325(3)
C-8*	24d	−0.0472(3)	−0.1673(3)	0.1828(3)
C-9*	24d	−0.0761(3)	−0.0806(3)	0.2269(3)
C-10*	24d	0.2352(3)	−0.0250(3)	0.0883(3)

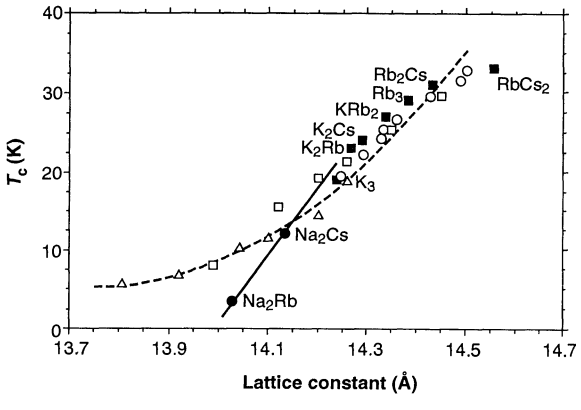

Fig. 4. Evolution of the critical temperature of superconducting fullerides with the cubic lattice constant. Filled symbols are ambient-pressure data (■ and ● for fcc and primitive cubic phases, respectively) from (*14*). Open symbols are both ambient-pressure data (○) from (*7*) and high-pressure data (□ for Rb_3C_{60} and △ for K_3C_{60}) from (*25*). The dotted line is the LDA calculation from (*23*) for fcc fullerides and the solid line is the present suggested behavior for primitive cubic systems.

estimated for K_3C_{60} (*21*). The order-disorder transition in Na_2MC_{60} is thus expected to be at a somewhat higher temperature than in pristine C_{60}. Differential scanning calorimetry (*22*) performed on Na_2CsC_{60} between 100 and 450 K confirmed the existence of an order-disorder phase transition at 299(3) K (change in enthalpy ΔH = 2.5(5) J/g).

The fcc merohedrally disordered superconducting $M_2M'C_{60}$ compounds obey a simple monotonic relation (*7*) between T_c and the cubic lattice constant a. Calculations (*23*) using the local density approximation (LDA) with varying a showed that T_c scales well with the density of states at the Fermi level, $N(\varepsilon_F)$. The position of Na_2CsC_{60}, which adopts a different structure on the universal curve, is thus wholly fortuitous (Fig. 4). Its "normal" behavior seems to indicate that there is little effect on $N(\varepsilon_F)$ arising from the strongly modified orientational potential. This lack of effect would disagree with the conclusions of tight-binding calculations (*4*), which indicate that $N(\varepsilon_F)$ is higher for the $Pa\bar{3}$ structure than for the $Fm\bar{3}m$ one. A strong possibility is then that the fortuitous position of Na_2CsC_{60} on the universal curve arises from the compensating effects of a slightly reduced electron-phonon coupling constant V, originating from the stronger influence of the Na^+ ions on the ball geometry. The unexpectedly low T_c of isostructural Na_2RbC_{60} should then result from a much steeper dependence of $N(\varepsilon_F)$ or V on the intermolecular separation (Fig. 4) in $Pa\bar{3}$ compared with $Fm\bar{3}m$. Detailed discussion has to await calculations in the primitive cubic structure as well as accurate structural parameters for other sodium and lithium ternary fullerides.

A theoretical understanding of how electron hopping between neighboring fullerene molecules is affected by their relative orientation in the context of the present experimental results is essential. Its effect on the details of the band structure will determine the extent to which interfullerene interactions contribute to the superconductivity mechanism in the fullerenes in addition to the intrafullerene interactions, which strongly contribute to the pair-binding (*5, 24*).

REFERENCES AND NOTES

1. A. F. Hebard *et al.*, *Nature* **350**, 600 (1991); K. Holczer *et al.*, *Science* **252**, 1154 (1991).
2. P. W. Stephens *et al.*, *Nature* **351**, 632 (1991).
3. M. P. Gelfand and J. P. Lu, *Phys. Rev. B* **46**, 4367 (1992); *Appl. Phys. A* **56**, 215 (1993); T. Yildirim, S. Hong, A. B. Harris, E. J. Mele, *Phys. Rev. B* **48**, 12262 (1993).
4. S. Satpathy *et al.*, *Phys. Rev. B* **46**, 1773 (1992).
5. C. M. Varma, J. Zaanen, K. Raghavachari, *Science* **254**, 989 (1991); M. Schluter, M. Lannoo, M. Needels, G. A. Baraff, D. Tomanek, *Phys. Rev. Lett.* **68**, 526 (1992); I. I. Mazin *et al.*, *Phys. Rev. B* **45**, 5114 (1992).
6. S. Chakravarty, M. P. Gelfand, S. Kivelson, *Science* **254**, 970 (1991).
7. R. M. Fleming *et al.*, *Nature* **352**, 787 (1991).
8. M. J. Rosseinsky *et al.*, *ibid.* **356**, 416 (1992).
9. K. Tanigaki *et al.*, *ibid.*, p. 419.
10. I. Hirosawa *et al.*, *Solid State Commun.* **87**, 945 (1993).
11. K. Kniaz *et al.*, *ibid.* **88**, 47 (1993).
12. T. Yildirim *et al.*, *Phys. Rev. Lett.* **71**, 1383 (1993).
13. R. Sachidanandam and A. B. Harris, *ibid.* **67**, 1467 (1991); W. I. F. David *et al.*, *Nature* **353**, 147 (1991); S. Liu, V.-J. Lu, M. M. Kappes, J. A. Ibers, *Science* **254**, 408 (1991).
14. K. Tanigaki *et al.*, *Europhys. Lett.* **23**, 57 (1993).
15. W. I. F. David, R. M. Ibberson, T. J. S. Dennis, J. P. Hare, K. Prassides, *ibid.* **18**, 219 (1992).
16. P. A. Heiney *et al.*, *Phys. Rev. Lett.* **66**, 2911 (1991).
17. P. C. Chow *et al.*, *ibid.* **69**, 2943 (1992).
18. P. W. Fowler, *Philos. Mag. Lett.* **66**, 277 (1992); W. Andreoni, in *Physics and Chemistry of the Fullerenes*, K. Prassides, Ed. (Kluwer Academic, Dordrecht, Netherlands, in press).
19. K. Prassides *et al.*, *Carbon* **30**, 1277 (1992).
20. C. Christides *et al.*, *Europhys. Lett.* **24**, 755 (1993).
21. C. Christides *et al.*, *Phys. Rev. B* **46**, 12088 (1992); S. E. Barrett and R. Tycko, *Phys. Rev. Lett.* **69**, 3754 (1992).
22. K. Tanigaki *et al.*, *Phys. Rev. B*, in press.
23. A. Oshiyama and S. Saito, *Solid State Commun.* **82**, 41 (1992).
24. K. Prassides *et al.*, *Nature* **354**, 462 (1991); *Europhys. Lett.* **19**, 629 (1992).
25. G. Sparn *et al.*, *Science* **252**, 1829 (1991); *Phys. Rev. Lett.* **68**, 1228 (1992).

26. We thank R. M. Ibberson for invaluable help with the experiments; W. Andreoni, A. Oshiyama, N. Hamada, and S. Saito for useful discussions; and the Science and Engineering Research Council, United Kingdom, for financial support and access to ISIS.

25 October 1993; accepted 6 December 1993

Increasing Turnover Through Time in Tropical Forests

O. L. Phillips and A. H. Gentry*

Tree turnover rates were assessed at 40 tropical forest sites. Averaged across inventoried forests, turnover, as measured by tree mortality and recruitment, has increased since the 1950s, with an apparent pantropical acceleration since 1980. Among 22 mature forest sites with two or more inventory periods, forest turnover also increased. The trend in forest dynamics may have profound effects on biological diversity.

Since the mid-20th century, a substantial body of data has been gathered on rates of tree mortality and recruitment ("turnover") in humid tropical forests. Turnover rates in mature tropical forests correlate with estimates of net productivity, as gauged by rates of basal area increment and mortality (*1–3*). Humid tropical forests are highly productive (*4, 5*), so proportional increases should be easier to detect in those systems than in temperate systems. Tropical forest study sites are also relatively secure from certain forms of anthropogenic atmospheric change such as acid precipitation (*6*), and their diversity buffers them against pathogen epidemics that can afflict temperate forests (*7*). Also, tropical forest inventory plots typically have no history of clear-felling or extractive logging; few temperate forests are old growth. Therefore, tropical forest turnover data may provide a novel test of the hypothesis that global forest productivity is increasing (*8*).

We compiled data on rates of tree turnover in tropical forests using logarithmic models to estimate annual mortality and recruitment rates (*2*). The evidence for directional change through time in tropical forest dynamics was evaluated by two methods. First, we used all forest dynamics data with ≥4 years of continuous measurement (mean, 13.3; median, 11.0; range, 4 to 38 years) and an area of ≥0.2 ha (mean, 2.7; median, 1.2; range, 0.2 to 23.5 ha) (Table 1) (*9*). Only forests known to have suffered mass mortality by deforestation, cyclones, drought, or flooding were excluded. The first long-term inventory that satisfied the criteria began in 1934, and measurements from the last were made as recently as 1993. The time between successive inventories of each plot was always >1 year; therefore, within each monitoring period we allocated the period's annualized turnover rate to each of the years included in the monitoring period. Using these estimates, we then compared turnover rates across all mature tropical forests through time and then separately for neotropical and paleotropical forests. Then, individual sites that have two or more successive inventory periods were used to test for temporal change within individual forests.

There has been a significant upward trend in average measured rates of turnover of tropical forest trees ≥10 cm in diameter since at least 1960 (*10*). One possible confounding factor is the tendency for early sites to be mostly paleotropical and for recent sites to be mostly neotropical. Within our data set, neotropical sites are more dynamic than paleotropical ones (*11*). Yet, when graphed separately both neotropical and paleotropical data sets continue to show significant increases in

Missouri Botanical Garden, Box 299, St. Louis, MO 63166, USA.

*1945–1993.